Determination of the Scaled Optical Thickness of Clouds from Reflected Solar Radiation Measurements

MICHAEL D. KING

Laboratory for Atmospheres, Goddard Space Flight Center, NASA, Greenbelt, MD 20771

(Manuscript received 29 September 1986, in final form 21 January 1987)

ABSTRACT

A method is presented for determining the scaled optical thickness of clouds from reflected solar radiation measurements. The procedure compares measurements of the reflection function with asymptotic expressions for the reflection function of optically thick layers. Analytic formulas are derived which explicitly show the dependence of the reflection and transmission functions of nonabsorbing atmospheres on cloud optical thickness (τ_c), ground albedo (A_g) and asymmetry factor (g). For nonconservative atmospheres, the dependence of the reflection function on single scattering albedo (ω_0) and asymmetry factor are contained implicitly in the asymptotic functions and constants. These asymptotic expressions for both conservative and nonconservative atmospheres are shown to be valid when the scaled optical thickness $(1 - g)\tau_c \geq 1.45$, corresponding to clouds of optical thickness $\tau_c \geq 9$. By utilizing the asymptotic expression for the reflection function of an optically thick, conservatively scattering atmosphere, a simple expression is obtained relating the measured reflection function to scaled optical thickness. This expression shows that the ground albedo produces a constant bias in the derived optical thickness, regardless of the value of the measured reflection function.

High-resolution images of the reflection function of clouds have been obtained with a multichannel scanning radiometer operated from a high-altitude aircraft. An image of the reflection function of clouds obtained from a stratiform cloud system in central Oklahoma is analyzed using two different phase functions. Results show that details of the single scattering phase function have an impact on the derived optical thickness, although the dominant influence is the cloud asymmetry factor which appears explicitly in the analysis.

1. Introduction

The reflection, transmission and absorption of radiation in a cloudy atmosphere is governed by the optical thickness, single scattering albedo and phase function of the cloud medium, as well as the albedo of the underlying surface. The possibility of using reflected solar radiation measurements from a high-altitude aircraft or satellite to derive the radiative properties of a cloudy atmosphere has long been recognized. Hansen and Pollack (1970) and Twomey and Cocks (1982) have used nadir observations of the spectral reflection function of clouds from aircraft to derive the optical thickness, mean particle radius and phase of the cloud particles. In addition, Twomey and Cocks compared in situ observations of the gross microphysical properties of clouds with those inferred from radiation measurements. These results have raised questions about our ability to remotely sense cloud radiative properties if the clouds are not horizontally homogeneous and if they are composed of substances other than pure water and water vapor. Rozenberg et al. (1974), Curran and Wu (1982) and Ahmad and Fraser (1983) have used spaceborne observations of the spectral reflection function of clouds to infer the cloud optical thickness. In none of these cases was it possible to verify the optical thickness or other derived properties of the clouds by in situ intercomparison.

The majority of cloud remote sensing studies to date have involved interpreting reflected solar radiation measurements using a large set of precomputed values of the reflection function for various solar zenith angles (θ_0), observational zenith angles (θ), relative azimuth angles (ϕ) and optical thicknesses (τ_c). These table look-up procedures are adequate, though time consuming, provided the computations pertain to the correct ground albedo (A_g) of the observations and use a reasonable representation of the cloud phase function. An alternative approach is to make use of asymptotic expressions for the reflection and transmission functions of optically thick layers in order to convert the radiation measurements to cloud optical thickness. Rozenberg et al. (1974) are the only previous investigators to have made use of these expressions in the interpretation of reflected solar radiation measurements from clouds.

The intent of this paper is to present a procedure for inferring the cloud optical thickness from reflected solar radiation measurements. This procedure is based on asymptotic expressions for the reflection and transmission functions of optically thick atmospheres. The range of optical thicknesses over which the asymptotic

expressions are valid, both for conservative and nonconservative atmospheres, will be discussed. In addition, the explicit dependence of the derived optical thickness on ground albedo and cloud asymmetry factor will be presented. An observational case of the reflection function of clouds obtained from high-altitude aircraft observations will be described. This image of the reflection function will be used to derive the cloud optical thickness using both a Mie theory phase function and a Henyey–Greenstein phase function having the same value of the asymmetry factor. This presentation highlights the effect of details of the phase function in obtaining accurate estimates of the cloud optical thickness. Since the cloud optical thickness depends on a combination of microphysical properties of the cloud, especially the vertically integrated liquid water content (liquid water path) and effective particle radius (Stephens, 1978), the cloud optical thickness does not give any single microphysical property of the cloud layer.

2. Reflection function of thick atmospheres

The diffusely reflected radiation at the top of the atmosphere and the diffusely transmitted radiation at the bottom of the atmosphere can be expressed in terms of the reflection function $R(\tau_c; \mu, \mu_0, \phi)$ and transmission function $T(\tau_c; \mu, \mu_0, \phi)$. In terms of these functions, the reflected $I(0, -\mu, \phi)$ and transmitted $I(\tau_c, \mu, \phi)$ intensities from a horizontally homogeneous atmosphere illuminated from above by a parallel beam of radiation of incident flux density F_0, may be expressed in the forms

$$I(0, -\mu, \phi) = (\mu_0 F_0/\pi) R(\tau_c; \mu, \mu_0, \phi), \quad (1)$$

$$I(\tau_c, \mu, \phi) = (\mu_0 F_0/\pi) T(\tau_c; \mu, \mu_0, \phi). \quad (2)$$

In these expressions, τ_c is the total optical thickness of the atmosphere (or cloud), μ_0 the cosine of the solar zenith angle, μ the absolute value of the cosine of the zenith angle, measured with respect to the positive τ direction, and ϕ the relative azimuth angle between the direction of propagation of the emerging radiation and the incident solar radiation ($0 \leqslant \mu, \mu_0 \leqslant 1$).

The reflection and transmission functions can be calculated using the doubling method (Hansen and Travis, 1974; van de Hulst, 1980). In this method, the reflection and transmission functions of a single layer of optical thickness $\tau_c/2$ are combined with a similar layer to obtain the reflection and transmission functions of a combined layer of optical thickness τ_c. Of the many different methods that have been used as initializations in the doubling method, we have chosen to obtain the reflection and transmission functions of the initial layer of infinitesimal optical thickness using the invariant imbedding initialization described by King (1983).

In the present investigation, two different phase functions have been employed in computations of the reflection and transmission functions of optically thick atmospheres. The first is a Mie phase function for a size distribution of particles of a given radius proportional to $r^6 \exp(-1.6187r)$, where r is the particle radius in μm. This distribution of particles is a gamma distribution with an effective radius of 5.56 μm and an effective variance of 0.111, and is typical of fair weather cumulus (FWC) clouds (Hansen, 1971). This distribution is similar to Deirmendjian's (1963) cloud C.1 model, except that the effective radius in Deirmendjian's model is 6.0 μm. The second phase function is the widely used analytic phase function first introduced by Henyey and Greenstein (1941) and given by

$$\Phi(\cos\Theta) = \frac{1 - g^2}{(1 + g^2 - 2g\cos\Theta)^{3/2}}, \quad (3)$$

where g is the asymmetry factor and Θ the scattering angle.

Figure 1 illustrates the reflection function as a function of τ_c for various values of the single scattering albedo ω_0, and for a model atmosphere which scatters radiation according to the Henyey–Greenstein phase function with $g = 0.85$. Results apply to nadir observations ($\mu = 1$) when the solar zenith angle $\theta_0 = 30°$ ($\mu_0 = 0.866$) and the ground albedo $A_g = 0$. The influence of surface reflection will be discussed in section 3. It is clear from Fig. 1, as well as from similar results presented by Twomey and Seton (1980), Curran et al. (1981) and Curran and Wu (1982), that measurements of the reflection function may be used to derive the optical thickness of clouds. The greatest sensitivity to optical thickness is seen to occur at wavelengths where absorption by clouds can be neglected ($\omega_0 \sim 1.0$) and where the cloud optical thickness lies in the range $7 \leqslant \tau_c \leqslant 70$. Furthermore, computational results show that the sensitivity of the reflection function to cloud optical thickness is the greatest for large values of μ_0 (e.g., see Curran et al., 1981).

When the optical thickness is sufficiently large, numerical results for the reflection and transmission functions must agree with known asymptotic expressions for very thick layers. In the case of conservative scattering ($\omega_0 = 1$), these expressions are given by (van de Hulst, 1980)

$$R_{\text{atm}}(\tau_c; \mu, \mu_0, \phi) = R_\infty(\mu, \mu_0, \phi) - \frac{4K(\mu)K(\mu_0)}{3(1-g)(\tau_c + 2q_0)}, \quad (4)$$

$$T_{\text{atm}}(\tau_c; \mu, \mu_0, \phi) = \frac{4K(\mu)K(\mu_0)}{3(1-g)(\tau_c + 2q_0)}, \quad (5)$$

where $R_\infty(\mu, \mu_0, \phi)$ is the reflection function of a semi-infinite atmosphere, $K(\mu)$ the escape function, and q_0 the extrapolation length for conservative scattering. The reduced extrapolation length $q' = (1 - g)q_0$ lies in the range 0.709 to 0.715 for all possible phase functions (van de Hulst, 1980), and thus the reflection and trans-

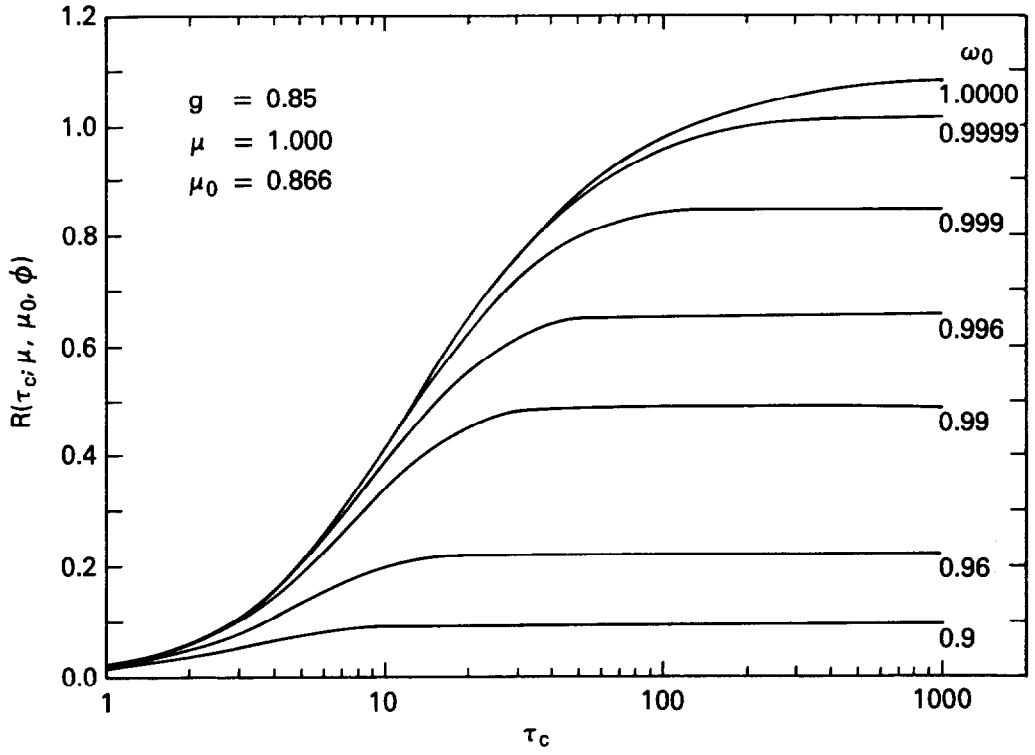

FIG. 1. Reflection function as a function of cloud optical thickness for a Henyey–Greenstein phase function with $g = 0.85$ and for seven values of the single scattering albedo. Results apply to nadir observations ($\mu = 1$) when the cosine of the solar zenith angle $\mu_0 = 0.866$ and the ground albedo $A_g = 0$.

mission functions for conservative scattering depend explicitly on the scaled optical thickness $(1 - g)\tau_c$ and implicitly on the phase function through its effect on $R_\infty(\mu, \mu_0, \phi)$ and $K(\mu)$.

For the case of nonconservative scattering ($\omega_0 < 1$), the reflection and transmission functions for optically thick atmospheres may be expressed as (van de Hulst, 1980)

$$R_{\text{atm}}(\tau_c; \mu, \mu_0, \phi) = R_\infty(\mu, \mu_0, \phi) - \frac{ml}{1 - l^2 e^{-2k\tau_c}} K(\mu)K(\mu_0)e^{-2k\tau_c}, \quad (6)$$

$$T_{\text{atm}}(\tau_c; \mu, \mu_0, \phi) = \frac{m}{1 - l^2 e^{-2k\tau_c}} K(\mu)K(\mu_0)e^{-k\tau_c}, \quad (7)$$

where k is the diffusion exponent describing the attenuation of radiation in the diffusion domain, and m and l constants which depend primarily on the single scattering albedo and asymmetry factor (King, 1981; King and Harshvardhan, 1986).

The functions and constants appearing in (4)–(7) can readily be determined by applying the asymptotic fitting method of van de Hulst (1968). Figure 2 illustrates the escape function as a function of μ and ω_0 for a model atmosphere having a Henyey–Greenstein phase function with $g = 0.85$. These results, together with (5) and (7), show that the transmitted radiation at the base of an optically thick atmosphere is *azimuthally independent* and four to seven times greater at the zenith ($\mu = 1$) than at the horizon ($\mu = 0$), depending on wavelength (and hence single scattering albedo). Comparable results can be found in King and Harshvardhan (1986) for the FWC phase function and for four values of the single scattering albedo.

For conservative scattering, the first and second moments of the escape function are given by

$$2\int_0^1 K(\mu)\mu d\mu = 1, \quad (8)$$

$$2\int_0^1 K(\mu)\mu^2 d\mu = (1 - g)q_0 = q'. \quad (9)$$

The relative insensitivity of the escape function to the high-order terms in the Legendre polynomial expansion of the phase function results in q' being nearly constant for all phase functions. King (1983) compared the escape function for the FWC and Henyey–Greenstein phase functions having the same asymmetry factor when $\omega_0 = 1$. The relative difference between these results is generally less than a few percent, though differences as large as 11% occur at the horizon.

The entire azimuthal dependence of the reflection function for thick atmospheres is contained in the re-

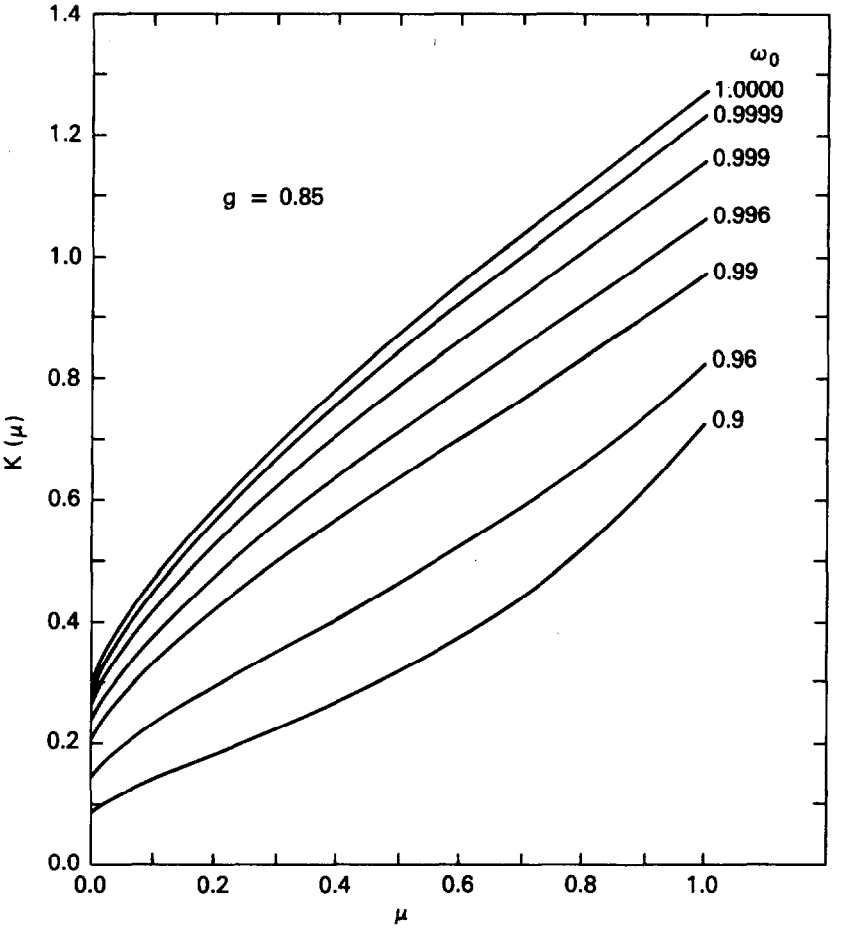

FIG. 2. Escape function as a function of cosine of the zenith angle for a Henyey–Greenstein phase function with $g = 0.85$ and for seven values of the single scattering albedo.

flection function for a semi-infinite atmosphere, which may be expressed as a Fourier expansion of the form

$$R_\infty(\mu, \mu_0, \phi) = R_\infty{}^0(\mu, \mu_0) + 2 \sum_{m=1}^{M(\mu,\mu_0)} R_\infty{}^m(\mu, \mu_0) \cos m\phi. \quad (10)$$

The variable upper limit $M(\mu, \mu_0)$ denotes the fact that the maximum number of terms required in the Fourier expansion of $R_\infty(\mu, \mu_0, \phi)$ depends on μ and μ_0. Both $M(\mu, \mu_0)$ and $R_\infty{}^m(\mu, \mu_0)$ are illustrated by King (1983) for the FWC and Henyey–Greenstein phase functions under the condition of conservative scattering. Contrary to the findings for $K(\mu)$ and q', $R_\infty{}^m(\mu, \mu_0)$ and $M(\mu, \mu_0)$ depend on details of the phase function. This is equally true for nonconservative scattering, where the constants k, l and m depend little on the higher order Legendre coefficients of the phase function (King, 1981; King and Harshvardhan, 1986), $K(\mu)$ depends somewhat on the details of the phase function, and $R_\infty{}^m(\mu, \mu_0)$ and $M(\mu, \mu_0)$ depend greatly on the details of the phase function.

3. Influence of surface reflection

The reflection and transmission functions in the earth-atmosphere system depend not only on the optical properties of the atmosphere, but also on the reflection properties of the surface. Assuming the atmosphere is vertically homogeneous with a surface that reflects radiation according to Lambert's law with some albedo A_g, it is well known that (Chandrasekhar, 1950)

$$R(\tau_c; \mu, \mu_0, \phi) = R_{\text{atm}}(\tau_c; \mu, \mu_0, \phi) + \frac{A_g}{1 - A_g \bar{r}_{\text{atm}}(\tau_c)} t_{\text{atm}}(\tau_c, \mu) t_{\text{atm}}(\tau_c, \mu_0), \quad (11)$$

$$T(\tau_c; \mu, \mu_0, \phi) = T_{\text{atm}}(\tau_c; \mu, \mu_0, \phi) + \frac{A_g}{1 - A_g \bar{r}_{\text{atm}}(\tau_c)} r_{\text{atm}}(\tau_c, \mu) t_{\text{atm}}(\tau_c, \mu_0). \quad (12)$$

In these expressions, $t_{\text{atm}}(\tau_c, \mu_0)$, $r_{\text{atm}}(\tau_c, \mu_0)$ and $\bar{r}_{\text{atm}}(\tau_c)$ are the total transmission (diffuse plus direct), plane albedo and spherical albedo when $A_g = 0$. The functions $t_{\text{atm}}(\tau_c, \mu_0)$, $r_{\text{atm}}(\tau_c, \mu_0)$ and $\bar{r}_{\text{atm}}(\tau_c)$, equivalent

to $\gamma_1(\tau_c, \mu_0)$, $s(\tau_c, \mu_0)/\mu_0$ and $\bar{s}$ in Chandrasekhar's notation, are given by the expressions

$$t_{atm}(\tau_c, \mu_0) = \frac{1}{\pi}\int_0^{2\pi}\int_0^1 T_{atm}(\tau_c; \mu, \mu_0, \phi)\mu d\mu d\phi + e^{-\tau_c/\mu_0}, \tag{13}$$

$$r_{atm}(\tau_c, \mu_0) = \frac{1}{\pi}\int_0^{2\pi}\int_0^1 R_{atm}(\tau_c; \mu, \mu_0, \phi)\mu d\mu d\phi, \tag{14}$$

$$\bar{r}_{atm}(\tau_c) = 2\int_0^1 r_{atm}(\tau_c, \mu_0)\mu_0 d\mu_0. \tag{15}$$

Though (11) and (12) apply to atmospheres of arbitrary optical thickness, the use of these expressions, together with (4)–(7), permit asymptotic expressions to be derived for the reflection and transmission functions of thick atmospheres overlaying a reflecting surface.

In order to derive asymptotic expressions for the functions $t_{atm}(\tau_c, \mu_0)$, $r_{atm}(\tau_c, \mu_0)$ and $\bar{r}_{atm}(\tau_c)$ which appear in (11) and (12), it is necessary to define the constant n as the μ weighted mean value of the escape function:

$$n = 2\int_0^1 K(\mu)\mu d\mu. \tag{16}$$

This constant, illustrated by King (1981) as a function of similarity parameter $s = [(1 - \omega_0)/(1 - \omega_0 g)]^{1/2}$, necessarily equals unity for conservative scattering (cf. Eq. 8). With this definition, it immediately follows, upon substituting (4)–(7) into (13)–(15), that asymptotic expressions for the total transmission, plane albedo and spherical albedo of thick layers are given by

$$t_{atm}(\tau_c, \mu_0) = \frac{4K(\mu_0)}{3(1-g)(\tau_c + 2q_0)}, \tag{17}$$

$$r_{atm}(\tau_c, \mu_0) = 1 - \frac{4K(\mu_0)}{3(1-g)(\tau_c + 2q_0)}, \tag{18}$$

$$\bar{r}_{atm}(\tau_c) = 1 - \frac{4}{3(1-g)(\tau_c + 2q_0)} \tag{19}$$

for conservative scattering and

$$t_{atm}(\tau_c, \mu_0) = \frac{mn}{1 - l^2 e^{-2k\tau_c}} K(\mu_0) e^{-k\tau_c}, \tag{20}$$

$$r_{atm}(\tau_c, \mu_0) = r_\infty(\mu_0) - \frac{mnl}{1 - l^2 e^{-2k\tau_c}} K(\mu_0) e^{-2k\tau_c}, \tag{21}$$

$$\bar{r}_{atm}(\tau_c) = A^* - \frac{mn^2 l}{1 - l^2 e^{-2k\tau_c}} e^{-2k\tau_c} \tag{22}$$

for nonconservative scattering. In these expressions, $r_\infty(\mu_0)$ is the plane albedo and $A^* = \bar{r}_\infty$ the spherical albedo of a semi-infinite atmosphere.

Substituting asymptotic expressions (4)–(7) and (17)–(22) into (11) and (12), it can be shown after some algebraic manipulation that the reflection and transmission functions for optically thick atmospheres overlaying a reflecting surface may be expressed in the form

$$R(\tau_c; \mu, \mu_0, \phi) = R_\infty(\mu, \mu_0, \phi) - \frac{4(1 - A_g)K(\mu)K(\mu_0)}{[3(1 - A_g)(1 - g)(\tau_c + 2q_0) + 4A_g]}, \tag{23}$$

$$T(\tau_c; \mu, \mu_0, \phi) = \frac{4K(\mu_0)[(1 - A_g)K(\mu) + A_g]}{[3(1 - A_g)(1 - g)(\tau_c + 2q_0) + 4A_g]} \tag{24}$$

when $\omega_0 = 1$ and

$$R(\tau_c; \mu, \mu_0, \phi) = R_\infty(\mu, \mu_0, \phi) - \frac{m[(1 - A_g A^*)l - A_g mn^2]K(\mu)K(\mu_0)e^{-2k\tau_c}}{[(1 - A_g A^*)(1 - l^2 e^{-2k\tau_c}) + A_g mn^2 l e^{-2k\tau_c}]}, \tag{25}$$

$$T(\tau_c; \mu, \mu_0, \phi) = \frac{m[(1 - A_g A^*)K(\mu) + A_g n r_\infty(\mu)]K(\mu_0)e^{-k\tau_c}}{[(1 - A_g A^*)(1 - l^2 e^{-2k\tau_c}) + A_g mn^2 l e^{-2k\tau_c}]} \tag{26}$$

when $\omega_0 < 1$. When $A_g = 0$, these expressions reduce to (4)–(7) and when $A_g = 1$ the reflection and transmission functions for an optically thick, conservatively scattering atmosphere become $R_\infty(\mu, \mu_0, \phi)$ and $K(\mu_0)$, respectively. The latter result, being independent of μ and ϕ, suggests that when $\omega_0 = 1$ the zenith angle dependence of transmitted radiation in a thick atmosphere becomes more nearly isotropic as the ground albedo increases, becoming isotropic in the limit of a ground albedo of unity.

Figures 3 and 4 illustrate $R(\tau_c; \mu, \mu_0, \phi)$ as a function of $(1 - g)\tau_c$ and A_g for the fair weather cumulus (FWC) model when $\mu = 1$ and $\mu_0 = 0.866$. These results, valid for water clouds at wavelengths of 0.754 μm (Fig. 3) and 1.626 μm (Fig. 4), were obtained by the doubling method using the exact expression (11) to allow for the influence of surface reflection at all values of τ_c. Both figures compare numerical computations (solid curves) with asymptotic expressions for thick layers (dashed curves), where Fig. 3 applies to conservative scattering ($\omega_0 = 1$) and Fig. 4 to nonconservative scattering ($\omega_0 = 0.99659$). The asymptotic functions $K(\mu)$, $R_\infty{}^m(\mu, \mu_0)$ and $M(\mu, \mu_0)$ which appear in (23), (24) and (10) are illustrated in King (1983) for the FWC and Henyey–Greenstein models at 0.754 μm. The asymptotic functions and constants appearing in (25) and (26) were obtained by the asymptotic fitting method of van de Hulst (1968, 1980).

From the comparisons illustrated in Figs. 3 and 4, asymptotic theory is seen to be accurate to within 1% for $(1 - g)\tau_c \geq 1.45$. Since the asymmetry factor in terrestrial clouds is approximately 0.84 in the midvisible region where $\omega_0 \sim 1$, asymptotic expressions (23) and (25) are valid for clouds of optical thickness $\tau_c \geq 9$.

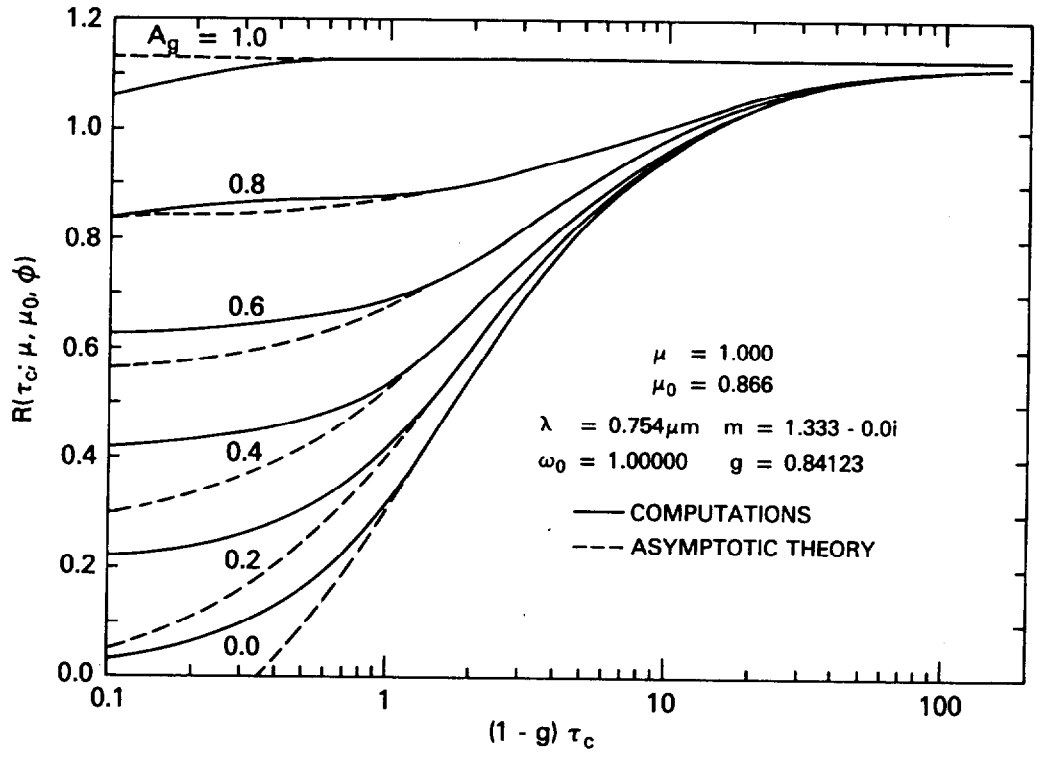

FIG. 3. Comparison of asymptotic theory with computations of the reflection function as a function of scaled optical thickness $(1 - g)\tau_c$ and ground albedo A_g for the fair weather cumulus (FWC) model at $\lambda = 0.754$ μm. Results apply to nadir observations ($\mu = 1$) when $\mu_0 = 0.866$.

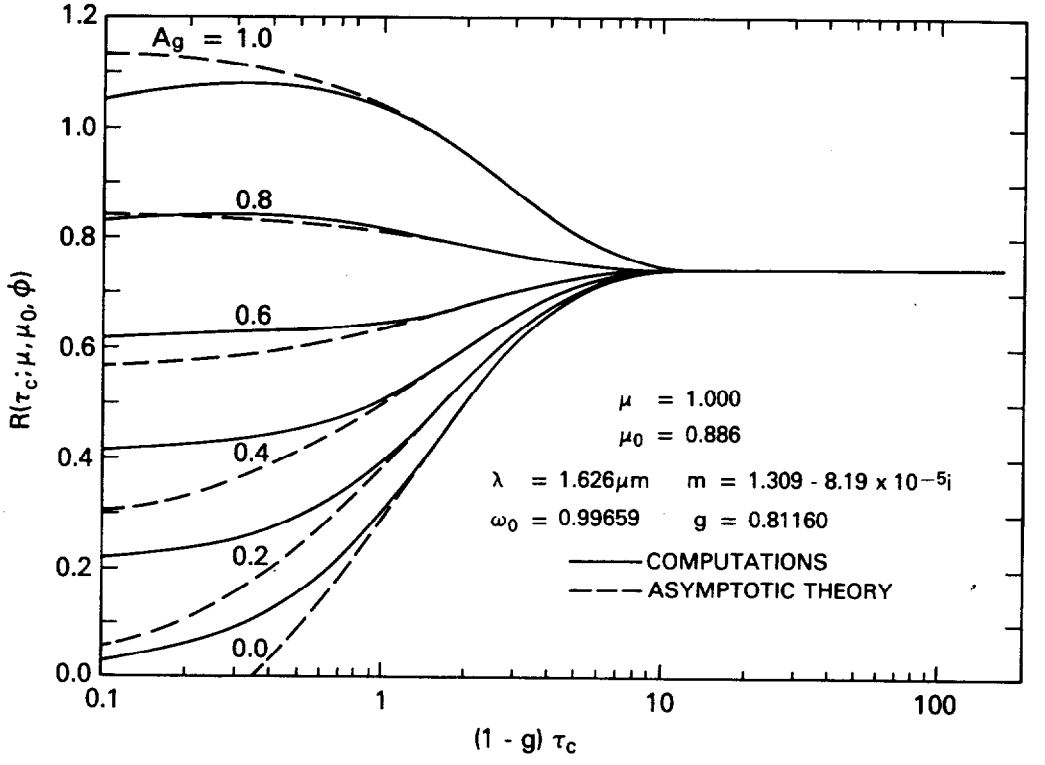

FIG. 4. As in Fig. 3, except for the FWC model at $\lambda = 1.626$ μm, where the refractive index of water is $1.309-8.19 \times 10^{-5}i$.

Although we have not examined the accuracy of the asymptotic theory expressions for the reflection function at all values of μ, μ_0 and ϕ, we have shown previously (King and Harshvardhan, 1986) that the asymptotic theory expressions for the plane albedo (Eqs. 18 and 21) are accurate for all values of μ_0 when $\tau_c \gtrsim 8$.

4. Determination of cloud optical thickness

From the results presented in Figs. 1, 3 and 4, it follows that the greatest sensitivity of the reflection function to cloud optical thickness occurs for conservative scattering when the underlying surface albedo is small. Furthermore, the optical thickness can best be determined for small values of the solar zenith angle when $1.2 \leqslant (1-g)\tau_c \leqslant 10$. Under these conditions, (23) describes the reflection function to an accuracy of better than 2%. Solving (23) for the scaled optical thickness τ_c' yields

$$\tau_c' = (1-g)\tau_c = \frac{4K(\mu)K(\mu_0)}{3[R_\infty(\mu,\mu_0,\phi) - R(\tau_c;\mu,\mu_0,\phi)]} - 2q' - \frac{4A_g}{3(1-A_g)}. \quad (27)$$

Thus, given a measurement $R_{\text{meas}}(\mu, \mu_0, \phi) = R(\tau_c; \mu, \mu_0, \phi)$, this expression shows that the scaled optical thickness of a cloud depends on q', A_g, $K(\mu)$ and the *difference* between $R_\infty(\mu, \mu_0, \phi)$ and the measured reflection function. The surface albedo and reduced extrapolation length enter this expression as offsets, independent of the magnitude of the reflection function. Measurements can therefore be analyzed assuming a value for A_g. If subsequent analysis shows the surface albedo to be different from the value previously assumed, a new scaled optical thickness can readily be determined by simply adjusting the values obtained from the earlier analysis.

In applying (27) to experimental measurements, it is necessary to estimate $K(\mu)$, $K(\mu_0)$ and $R_\infty(\mu, \mu_0, \phi)$ for each pixel. King (1983) has presented computations of $K(\mu)$, $R_\infty{}^m(\mu, \mu_0)$ and $M(\mu, \mu_0)$ for the FWC cloud model at a wavelength of 0.754 μm. This wavelength, corresponding to channel 1 of the multichannel cloud radiometer described by Curran et al. (1981), is a wavelength for which absorption due to water vapor, oxygen and liquid (or ice) particles is assumed to be negligible. These results have been compared with those for an atmosphere having a Henyey–Greenstein phase function with the same asymmetry factor ($g = 0.841$) as in the cloud model. The relative differences in the escape function and azimuthally independent reflection function are generally less than a few percent, although differences as large as 70% occur in the reflection function at angles where single scattering is important ($\mu = \mu_0 \sim 0$). The azimuth-dependent terms of the reflection function are generally dissimilar, with generally more terms required in the Fourier expansion of the reflection function for a FWC phase function than for a Henyey–Greenstein phase function.

As a consequence of the dependence of $R_\infty(\mu, \mu_0, \phi)$ and, to a much lesser extent, $K(\mu)$, on the higher order moments of the phase function, the scaled optical thickness derived from reflected solar radiation measurements will depend on the phase function assumed in the analysis. A similar conclusion was reached by Malkova (1973), who noted that the uncertainty in the phase function of the clouds being observed could lead to an uncertainty in τ_c of approximately 2. Although a large portion of this uncertainty results from the uncertainty in the asymmetry factor, Malkova further noted the potentially large influence of the phase function on the reflection function of a semi-infinite atmosphere $R_\infty(\mu, \mu_0, \phi)$. This effect will be demonstrated in the following sections, where aircraft observations are analyzed using both the FWC and Henyey–Greenstein phase functions with the same value of the asymmetry factor.

In addition to the phase function, the scaled optical thickness derived from reflected solar radiation measurements depends on the single scattering albedo assumed in the analysis. Although we will assume conservative scattering in the analysis of our reflected solar radiation measurements, (25) permits us to examine the uncertainty in the scaled optical thickness arising from this assumption. Thus, for nonconservative scattering,

$$\tau_c' = \frac{(1-g)}{2k}\ln\left\{\left[l - \frac{A_g m n^2}{(1-A_g A^*)}\right] \times \left[\frac{mK(\mu)K(\mu_0)}{[R_\infty(\mu,\mu_0,\phi) - R(\tau_c;\mu,\mu_0,\phi)]} + l\right]\right\}. \quad (28)$$

Since the logarithm of a product equals the sum of the logarithms, this expression shows once again that the surface albedo produces a constant bias in the derived optical thickness, regardless of the magnitude of the reflection function.

Each of the functions and constants appearing in (28) can be written in the form of a power series expansion in k (van de Hulst, 1980) such that

$$m = \frac{8}{3(1-g)}k + O(k^3), \quad (29)$$

$$l = 1 - 2q_0 k + 2q_0{}^2 k^2 + O(k^3), \quad (30)$$

$$n = 1 - q_0 k + O(k^2), \quad (31)$$

$$A^* = 1 - \frac{4(1-q_0 k)}{3(1-g)}k + O(k^3), \quad (32)$$

$$K(\mu) = (1-q_0 k)K(1;\mu) + O(k^2), \quad (33)$$

$$R_\infty(\mu,\mu_0,\phi) = R_\infty(1;\mu,\mu_0,\phi) - \frac{4k}{3(1-g)}K(1;\mu)K(1;\mu_0) + O(k^2), \quad (34)$$

where $O(k^2)$ denotes terms of order k^2 or higher, and $K(1;\mu)$ and $R_\infty(1;\mu,\mu_0,\phi)$ denote the escape function and reflection function of a semi-infinite atmosphere for conservative scattering ($\omega_0 = 1$). The diffusion exponent k can be evaluated in terms of the single scattering albedo and asymmetry factor as

$$k = [3(1-\omega_0)(1-\omega_0 g)]^{1/2} + O(1-\omega_0). \quad (35)$$

Although (28) is accurate for all values of ω_0, (29)–(35) are the most accurate for small values of k (i.e., $\omega_0 \geq 0.995$). Analytic approximations for k, m, l, n and A^* applicable over the full range $0 \leq \omega_0 \leq 1$ can be found elsewhere (King, 1981; King and Harshvardhan, 1986).

5. Error analysis

Having determined the scaled optical thickness from (27), it is important to examine the overall uncertainty in τ_c'. Uncertainties in τ_c' arise as a result of measurement errors in the reflection function (ΔR_{meas}), as well as from modeling errors associated with uncertainties in the surface albedo (ΔA_g), phase function and single scattering albedo. As pointed out previously, the major consequence of an uncertainty in the phase function is the resulting uncertainty in $R_\infty(1;\mu,\mu_0,\phi)$, the reflection function of a conservatively scattering, semi-infinite atmosphere (ΔR_∞). The uncertainty in the single scattering albedo is equivalent to an uncertainty in the diffusion exponent (Δk), which in turn leads to an uncertainty in $R_\infty(\mu,\mu_0,\phi)$ according to (34). It therefore follows from the method of propagation of errors (Bevington, 1969) that the uncertainty in the scaled optical thickness ($\Delta\tau_c'$) may be obtained from the expression

$$\Delta\tau_c' = \left(\frac{\partial\tau_c'}{\partial R_{meas}}\right)_{A_g,R_\infty,k}\Delta R_{meas} + \left(\frac{\partial\tau_c'}{\partial A_g}\right)_{R_{meas},R_\infty,k}\Delta A_g + \left(\frac{\partial\tau_c'}{\partial R_\infty}\right)_{R_{meas},A_g,k}\Delta R_\infty + \left(\frac{\partial\tau_c'}{\partial k}\right)_{R_{meas},A_g,R_\infty}\Delta k. \quad (36)$$

The first three partial derivatives appearing on the right-hand side of this expression can readily be evaluated using (27), resulting in

$$\Delta\tau_c' = \frac{4K(\mu)K(\mu_0)}{3[R_\infty(\mu,\mu_0,\phi) - R_{meas}(\mu,\mu_0,\phi)]^2}\times[\Delta R_{meas} - \Delta R_\infty] - \frac{4}{3(1-A_g)^2}\Delta A_g + \left(\frac{\partial\tau_c'}{\partial k}\right)_{R_{meas},A_g,R_\infty}\Delta k. \quad (37)$$

The final partial derivative requires the use of (28), where $R_{meas}(\mu,\mu_0,\phi)$, A_g and $R_\infty(1;\mu,\mu_0,\phi)$ are held constant. Taking the partial derivative of (28) with respect to R and substituting (29)–(34) into the resulting expression, it can be shown after considerable algebraic manipulation that

$$\left(\frac{\partial\tau_c'}{\partial k}\right)_{R_{meas},A_g,R_\infty} = O(k), \quad (38)$$

where the exact form of the coefficients of order k involve solutions of new integral equations not previously defined. Equations (37) and (38) nevertheless imply that

$$\tau_c' = \tau_c'(\omega_0 = 1) + O(k^2). \quad (39)$$

Over a low albedo surface the second term in (37) is small, as expected, though it can become quite large over a high albedo surface (cf. Fig. 3). Similarly, the uncertainty in τ_c' arising from the first term becomes progressively larger as the measured reflection function approaches that of a semi-infinite atmosphere. The only subtlety worth noting in (37) is that associated with solar zenith angle. Since the error in the first term goes as $K(\mu_0)$, one might expect that the error in the derived optical thickness would be the largest when μ_0, and hence $K(\mu_0)$, is the largest. That this is not the case is easily seen from the fact that as μ_0 decreases, the reflection function of a semi-infinite atmosphere becomes so small that the difference $[R_\infty(\mu,\mu_0,\phi) - R_{meas}(\mu,\mu_0,\phi)]$ becomes small. This causes the error in the derived value of τ_c' to increase as μ_0 decreases.

Table 1 provides a summary of the values of cloud optical thickness that would be derived for various values of the measured reflection function $R_{meas}(\mu,\mu_0,\phi)$, where we assumed the FWC model with $\mu = 1$ and $\mu_0 = 0.87178$. The values of cloud optical thickness presented in this table were obtained using (27) when $\omega_0 = 1$ and (28)–(35) when $\omega_0 < 1$. In all experimental results presented later, we assumed the surface albedo $A_g = 0.2$. As shown in (27) and (28), the surface albedo produces a constant offset in the derived value of the cloud optical thickness, regardless of the magnitude of the measured reflection function. For all three single scattering albedos considered here (viz., 1.0, 0.9999 and 0.9998), a surface albedo of 0.0 is seen to increase the optical thickness one would derive for $A_g = 0.2$ by $\Delta\tau_c = 2.1$ ($\Delta\tau_c' = 0.33$). A nonunity single-scattering albedo, on the other hand, increases the optical thickness that would be derived for a given value of the measured reflection function. Both from Fig. 1 and Table 1 we see that the single-scattering albedo produces a bias in the derived value of the cloud optical thickness which *increases* as the measured reflection function (and hence optical thickness) increases. This bias is roughly linear in $(1-\omega_0)$ for small to moderate values of τ_c, as predicted by (39).

TABLE 1. Values of the cloud optical thickness τ_c that would be obtained as a function of the measured reflection function $R_{meas}(\mu, \mu_0, \phi)$ for various values of the single scattering albedo and ground albedo.*

Reflection function	$\omega_0 = 1.0$		$\omega_0 = 0.9999$		$\omega_0 = 0.9998$	
	$A_g = 0.0$	$A_g = 0.2$	$A_g = 0.0$	$A_g = 0.2$	$A_g = 0.0$	$A_g = 0.2$
0.53182	12.10	10.00	12.24	10.14	12.39	10.29
0.72392	22.10	20.00	22.58	20.48	23.09	20.99
0.82255	32.10	30.00	33.24	31.14	34.51	32.42
0.88259	42.10	40.00	44.37	42.27	47.08	44.98
0.92297	52.10	50.00	56.14	54.04	61.40	59.30
0.95199	62.10	60.00	68.78	66.68	78.63	76.53
0.97386	72.10	70.00	82.61	80.51	101.20	99.11
0.99092	82.10	80.00	98.10	96.00	136.37	134.28
1.00461	92.10	90.00	116.01	113.91	249.71	247.61
1.01584	102.10	100.00	137.69	135.59	—	—

* All computations were performed assuming the fair weather cumulus (FWC) model when $\mu = 1.0$ and $\mu_0 = 0.87178$. For these conditions, $R_\infty(1; \mu, \mu_0, \phi) = 1.12933$, $K(1; \mu) = 1.27808$, $K(1; \mu_0) = 1.17482$, $q_0 = 4.50199$ and $g = 0.84123$.

6. Aircraft observations

a. Instrumentation

The Goddard multichannel cloud radiometer is a seven-channel scanning radiometer whose band center and bandwidth characteristics are summarized in Table 2. This instrument, shown in Fig. 5, was designed to operate from a high-altitude research aircraft and to scan the scene below the aircraft in a plane perpendicular to the velocity vector of the aircraft. The measurements reported in this paper were acquired from the NASA WB-57F aircraft. This aircraft, as well as the NASA ER-2 aircraft used from 1983–present, flies at a nominal altitude of 19 km, well above the highest cirrus and cumulonimbus clouds. The cloud radiometer has flown as one of a cluster of instruments, including a passive microwave radiometer (Wang et al., 1983) and nadir-viewing lidar (Spinhirne et al., 1982, 1983).

The upwelling radiation from the earth–atmosphere system is first reflected from a rotating scan mirror canted 45° to the long axis of the instrument (cf. Fig. 5). After being reflected by the scan mirror, the radiation is collected by a Dall-Kirkham (Cassegrainian) telescope which defines the field of view of the instrument at 7 mrad. Following transmission through the telescope the radiation next encounters a complex configuration of dichroic beam splitters, mirrors, lenses, interference filters and a prism (see Curran et al., 1981). This enables all seven channels of the cloud radiometer to be sampled simultaneously. Figures 3 and 4, which illustrate the sensitivity of the reflection function to cloud optical thickness and surface albedo for water clouds at 0.754 and 1.626 μm, correspond to expected measurements for nadir observations in channels 1 and 5 of the cloud radiometer.

TABLE 2. Spectral characteristics of the multichannel cloud radiometer during the June 1979 SESAME experiment.

Channel	Central wavelength (μm)	Spectral resolution (μm)
1	0.7540	0.0014
2	0.7609	0.0014
3	0.7631	0.0014
4	1.139	0.080
5	1.626	0.078
6	2.165	0.115
7	10.757	0.911

The electronics subsystem, in addition to providing aircraft power conversion and detector amplification, supplies heat to several temperature-critical elements of the scanner and produces reference voltages in steps from 0 to 4.5 V. Digital data are then pulse code modulated and recorded on analog flight tapes together with time and scan count number. The reference voltage levels in the data stream allow subsequent conversion of instrument data from digital counts to voltage.

Radiometric calibration of the first six channels is obtained by observing the output of a 182.5 cm integrating sphere maintained at Goddard Space Flight Center. The highly lambertian radiation exiting a 25 cm opening on the side of the sphere illuminates a 45° inclined mirror which reflects radiation upward to the multichannel cloud radiometer. The output voltage in each channel is then measured as a function of spectral intensity for varying illumination levels from the sphere. Since the sphere calibration of the radiometer includes throughput of the entire optical system, plus highly reflecting calibration mirror, the radiometric calibration of channel 1 is expected to be near that of the sphere calibration itself, estimated to be somewhat better than ±4% (Curran et al., 1981).

b. Geometric considerations

In order to determine the scaled optical thickness of clouds using (27), it is necessary to determine μ_0, μ

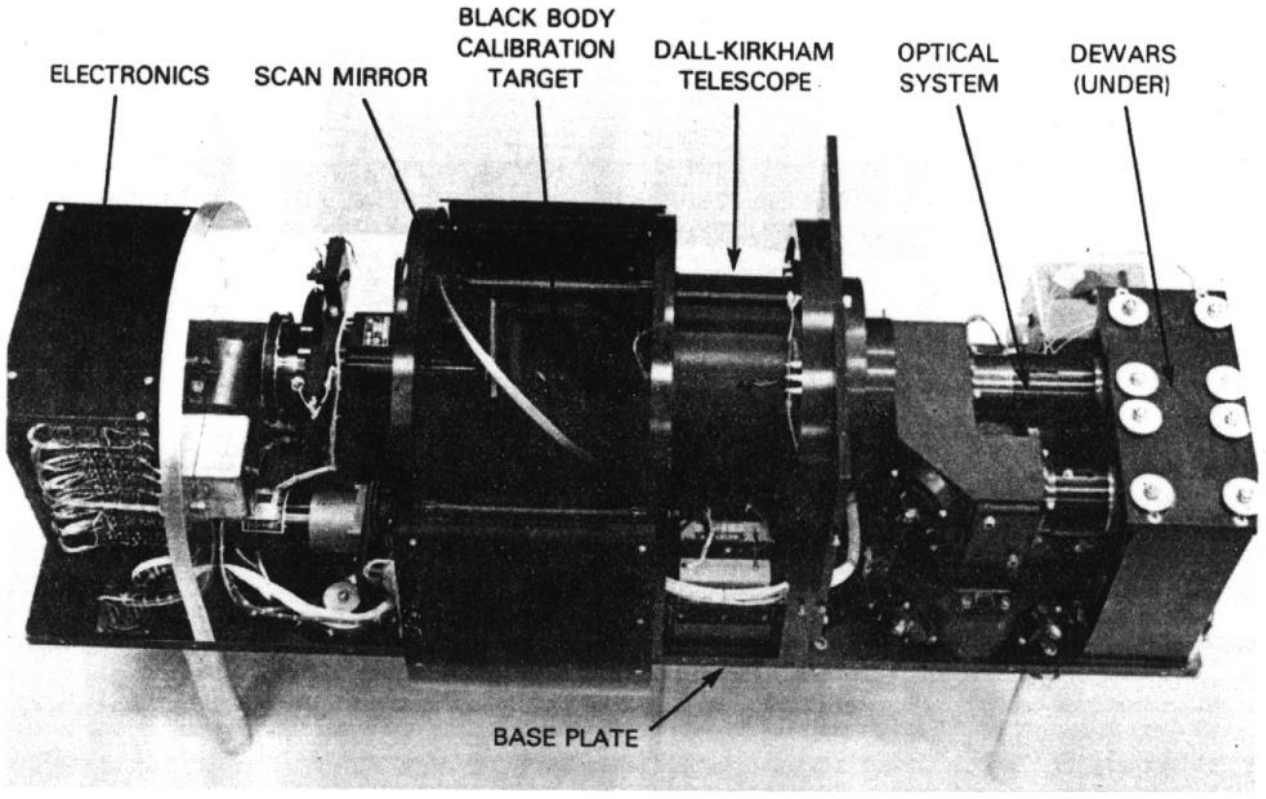

FIG. 5. Multichannel scanning radiometer used to measure the spectral reflectance of clouds.

and ϕ for each pixel. The solar zenith angle θ_0 and azimuth angle of the sun relative to north, denoted ϕ_0, must first be determined given the latitude, longitude and time of the observations. The observational zenith angle θ and relative azimuth angle ϕ depend, in addition, on the aircraft pitch (p), roll (r) and heading (H). Referring to Fig. 6, one can easily show that

$$\mu = \cos\theta = \cos p \cos(r+\alpha), \tag{40}$$

where α is the scan angle of the cloud radiometer relative to aircraft nadir. The angles appearing in this expression are defined as positive for the case illustrated in Fig. 6, where the aircraft nose is pitched upward, the aircraft is banking (rolling) to the right, and the pixel being observed is to the left of the aircraft nadir. Since the scan mirror of the cloud radiometer rotates in a counterclockwise direction, the pixels being observed during each active scan interval decrease from $\alpha = 45°$ to $\alpha = -45°$.

The relative azimuth angle between the direction of propagation of the reflected radiation and the incident solar direction is given by

$$\phi = H - \frac{\pi}{2} + \beta - \phi_0, \tag{41}$$

where both H and ϕ_0 are measured clockwise from north. With this definition and with reference to Fig. 6, one can see that ϕ is taken as 0° for forward reflection and 180° for backward reflection. The azimuth angle β which appears in this expression may be computed given the nadir scan angle of the instrument and the pitch and roll of the aircraft. Thus, referring to Fig. 6, it can be shown that

$$\tan\beta = \sin p \operatorname{ctn}(r+\alpha), \tag{42}$$

where β is to be taken in the interval $0 \leqslant \beta \leqslant \pi$. Only when $p = 0$ is the redundant solution $\tan\beta = 0$ obtained. In this situation it is obvious that β equals 0 when α is positive and π when α is negative.

All aircraft ephemeris (navigation) data were obtained from an inertial navigation system (INS) aboard the aircraft. These data were sampled and digitized every 4 s and subsequently merged with digital data from the multichannel cloud radiometer. Since the scan rate of the cloud radiometer is 3.47 Hz, corresponding to a scan duration of 288 ms, the INS data were interpolated to provide one set of ephemeris data per scan of the radiometer.

7. Results from observations

In May–June 1979, multichannel cloud radiometer observations were made in the vicinity of central Okla-

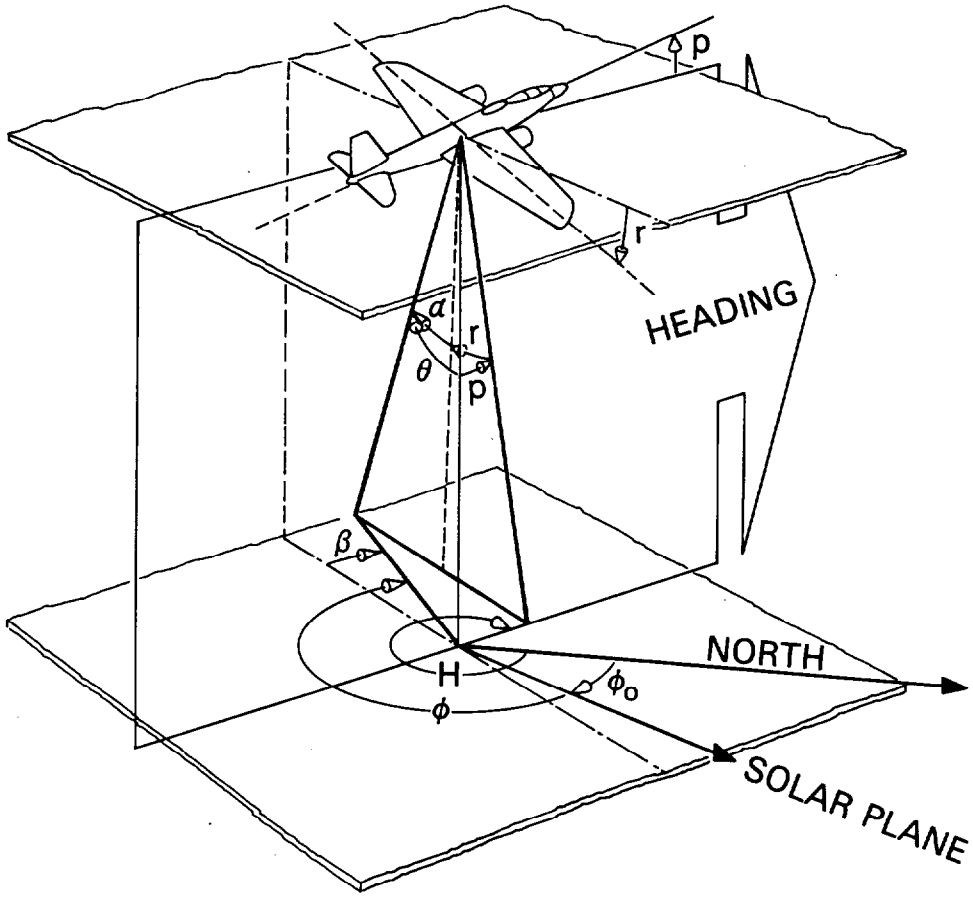

FIG. 6. Schematic illustration of the relationship between the zenith angle θ and relative azimuth angle ϕ of radiation reflected by the earth-atmosphere system, and the heading H, roll r, pitch p and nadir viewing angle α of the aircraft.

homa as part of the Severe Environmental Storms and Mesoscale Experiment (SESAME). On 8 June, a frontal system with associated optically thick clouds and embedded thunderstorms was located throughout much of Oklahoma and Kansas. During this day a number of NW–SE flight lines were flown over the cloud system between the frontal boundary and the optically thick cloud system to the northwest of the front. Figure 7 illustrates a GOES-West visible image taken at 2017 UTC on this day, upon which is superimposed the location and direction of flight of aircraft flight line 2. This flight line, to be discussed later, coincides closest in time to the GOES-West satellite image. The latitude and longitude grid in Fig. 7 applies to an altitude of 10 km, corresponding roughly to the cloud top altitude of the majority of clouds in the scene. The state boundaries shown in Fig. 7 apply to the surface, thus accounting for the parallax displacement between the state boundaries and latitude grid evident in the figure.

Figure 8 illustrates measurements of the reflection function for scan line 165 of the cloud radiometer on 8 June at a wavelength of 0.754 μm, where we converted the calibrated measurements of reflected intensity to reflection function using (1). In order to convert these measurements of $R_{\text{meas}}(\mu, \mu_0, \phi)$ to scaled optical thickness using (27), it is necessary to have an estimate of $R_\infty(\mu, \mu_0, \phi)$, $K(\mu)$ and q' for the cloud scene being observed, as well as an estimate of A_g for the surface beneath the cloud layer.

Figure 9 illustrates the reflection function of a semi-infinite atmosphere as a function of θ and ϕ for the FWC and Henyey–Greenstein phase functions when the solar zenith angle $\theta_0 = 29.5°$, corresponding to the time of the radiometer observations presented in Fig. 8. These polar diagrams, constructed using the azimuth-dependent reflection functions together with the Fourier expansion given by (10), show a dramatic difference in the reflection function of a semi-infinite atmosphere for different phase functions having the same value of the asymmetry factor. This is especially true in the principal plane, where the FWC phase function (Fig. 9a) results in enhanced reflection in the glory region ($\phi = 180°$) and a forward reflection lobe ($\phi = 0°$) substantially displaced from that for the Henyey–

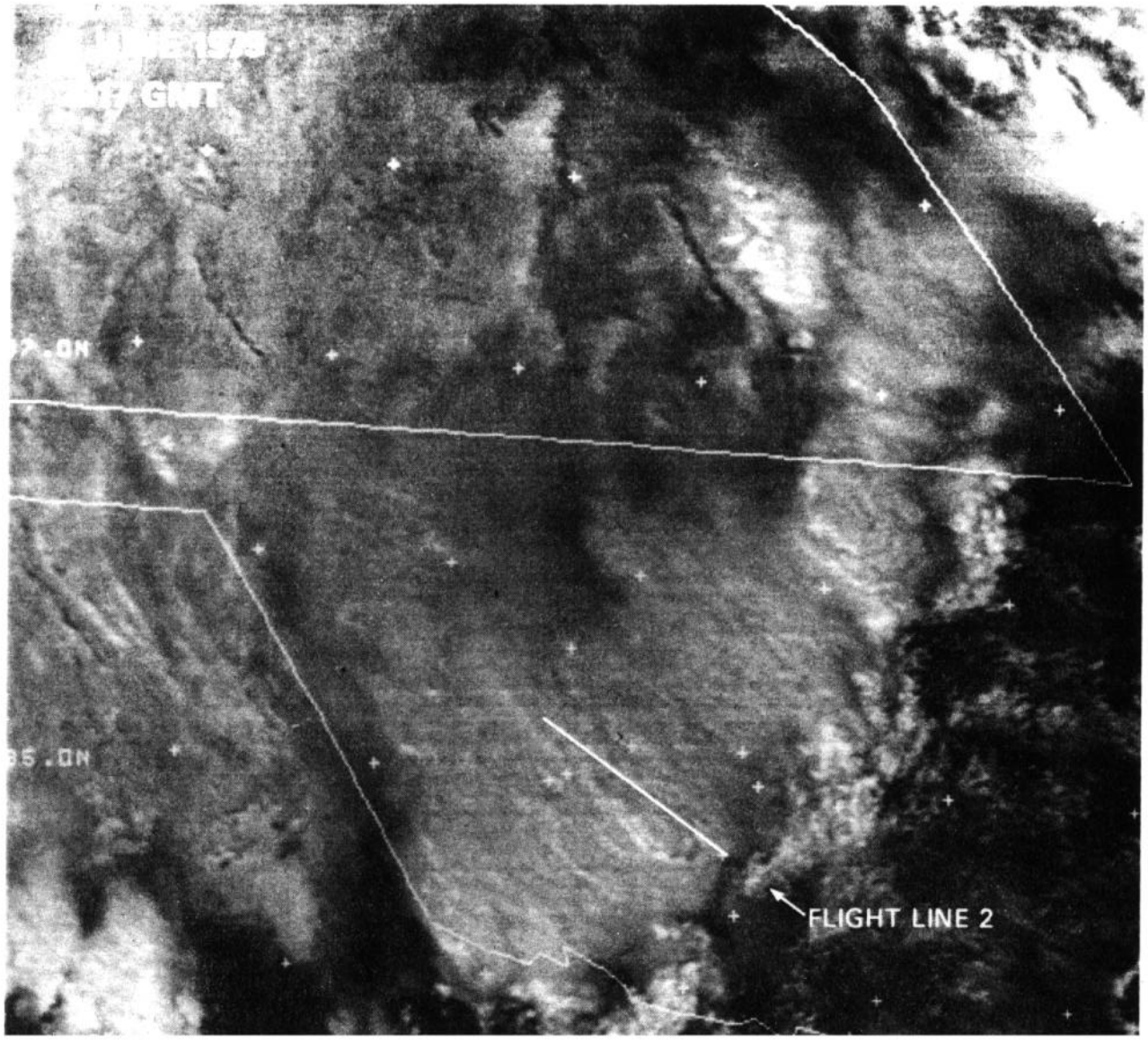

FIG. 7. GOES West visible image for 2017 UTC on 8 June 1979. The image encompasses the central Oklahoma area covered by the cloud radiometer measurements, and includes the flight track of the observations. The arrow denotes the direction of flight.

Greenstein model (Fig. 9b). The dotted line superimposed on Figs. 9a and b corresponds to scan line 165 of the cloud radiometer, at which time the aircraft was pitched upward ($p = 1.8°$) and heading in a direction of 69° relative to the solar direction. The fact that the aircraft scan does not go through local nadir, but is displaced toward the direction of flight, is a direct consequence of positive aircraft pitch. Due to aircraft roll to the left ($r = -1.2°$), one sees that the zenith angles covered by the measurements on this scan line range from somewhat less than 45° on the left-hand side of the aircraft to somewhat greater than 45° on the right-hand side of the aircraft. Note that the polar diagrams illustrated in Fig. 9 extend only to 50°.

The values of $R_\infty(\mu, \mu_0, \phi)$ derived from Fig. 9 for the θ and ϕ angles of each pixel are illustrated in Fig. 8. The relatively large difference in these two theoretical functions is partly a result of the fact that the scan line lies near the principal plane. Figures 8 and 9 clearly show that the details of the phase function, and not just the value of the asymmetry factor, affect radiative transfer computations of the intensity field, even in semi-infinite atmospheres. Figure 8 further suggests that very large differences should be expected in the derived values of the scaled optical thickness, depending on which model is assumed in the analysis.

Figure 10 illustrates the derived cloud optical thickness for the scan line presented in Fig. 8. In this and

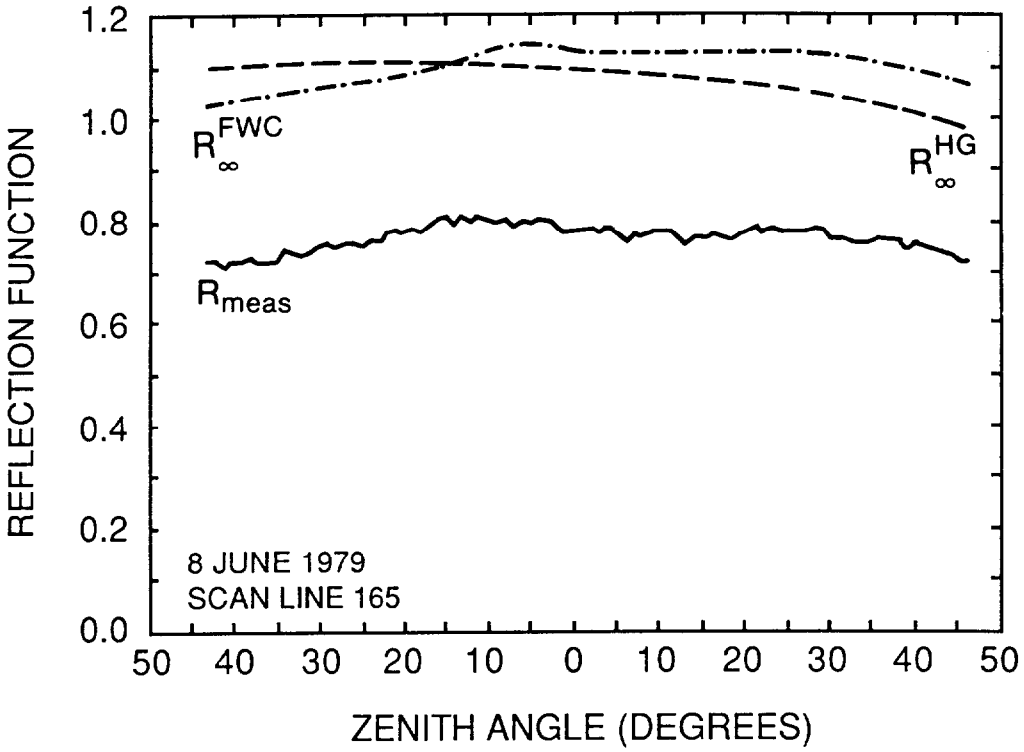

FIG. 8. Comparison of the measured reflection function (R_{meas}) and theoretical reflection function for a semi-infinite atmosphere (R_∞) as a function of zenith angle for scan line 165 of the cloud radiometer on 8 June 1979, flight line 2. Theoretical values of R_∞ are presented for both the FWC and Henyey–Greenstein models. All measurements apply at 0.754 μm.

succeeding figures, the scaled optical thickness τ_c' has been converted to optical thickness τ_c by assuming the asymmetry factor $g = 0.841$. For water clouds in the visible wavelength region, the asymmetry factor lies in the range $0.8 \leqslant g \leqslant 0.884$, with large (small) values associated with large (small) values of the effective radius of the droplet size distribution. Our assumption that the cloud scatters radiation according to Mie theory with a FWC size distribution leads to the inferred cloud optical thickness being the greatest on the left-hand side of the scan. In contrast, our assumption of a Henyey–Greenstein phase function for the scattering process results in the inferred optical thickness being the greatest on the right-hand side of the scan. These results are a direct consequence of differences in the theoretical values of $R_\infty(\mu, \mu_0, \phi)$, for (27) shows that the scaled optical thickness (and hence optical thickness) is directly related to the *difference* between $R_{meas}(\mu, \mu_0, \phi)$ and $R_\infty(\mu, \mu_0, \phi)$. This is especially true since $K(\mu)$ and q' are virtually indistinguishable for phase functions having the same value of the asymmetry factor (King, 1983). Note further that, although the difference in $R_\infty(\mu, \mu_0, \phi)$ for the two models illustrated in Fig. 8 is generally within 10%, the differences in the resulting values of τ_c' in Fig. 10 are as much as 50% owing to the dependence of τ_c' on the difference between $R_{meas}(\mu, \mu_0, \phi)$ and $R_\infty(\mu, \mu_0, \phi)$.

We have applied the techniques described heretofore to the first 365 scan lines of cloud radiometer data obtained on 8 June 1979, flight line 2. Figure 11 illustrates images of the measured reflection function and corresponding cloud optical thickness derived by assuming either the FWC or Henyey–Greenstein phase functions in the analysis. In all of these images, the aircraft was flying from top to bottom down the center of the images with the cloud radiometer scanning counterclockwise. All of these images have been remapped onto a horizontal grid at 10 km altitude, thus providing a uniform spatial scale.

Comparing the reflection function image of Fig. 11 with the GOES-West image of Fig. 7, one sees that the reflection function increases across the frontal boundary from about 0.5 to 0.8 or more. Beyond scan line 365, the cloud system contained embedded thunderstorms with overshooting tops, and thus data from this portion of the flight were unsuitable for further analysis. This portion of the cloud system has considerable variation in the reflection function resulting from the highly structured upper cloud boundary. This in turn resulted in many bright and dark (shadow) regions with meaningless optical thickness results. In contrast, the data presented in Fig. 11 correspond to a well-defined extended cloud layer with a relatively smooth upper boundary, thus enabling the cloud optical thickness to

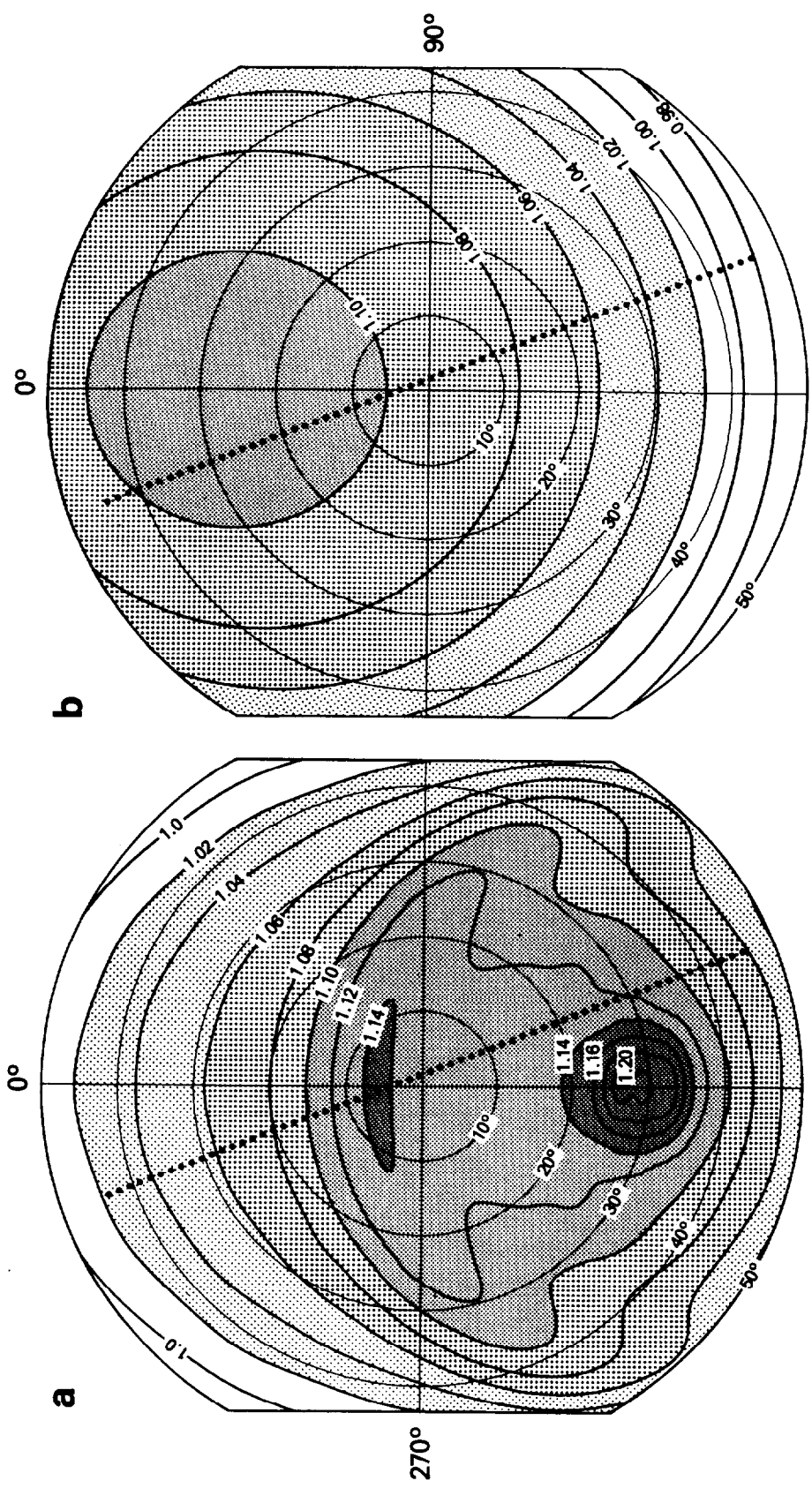

FIG. 9. Computations of the reflection function of a semi-infinite atmosphere $R_\infty(\mu, \mu_0, \phi)$ as a function of θ and ϕ for the (a) FWC and (b) Henyey–Greenstein phase functions when θ_0 = 29.5°. The dotted line superimposed on these figures corresponds to scan line 165 of the cloud radiometer on 8 June 1979, flight line 2. At this time the aircraft was heading in a direction of 69° relative to the solar direction.

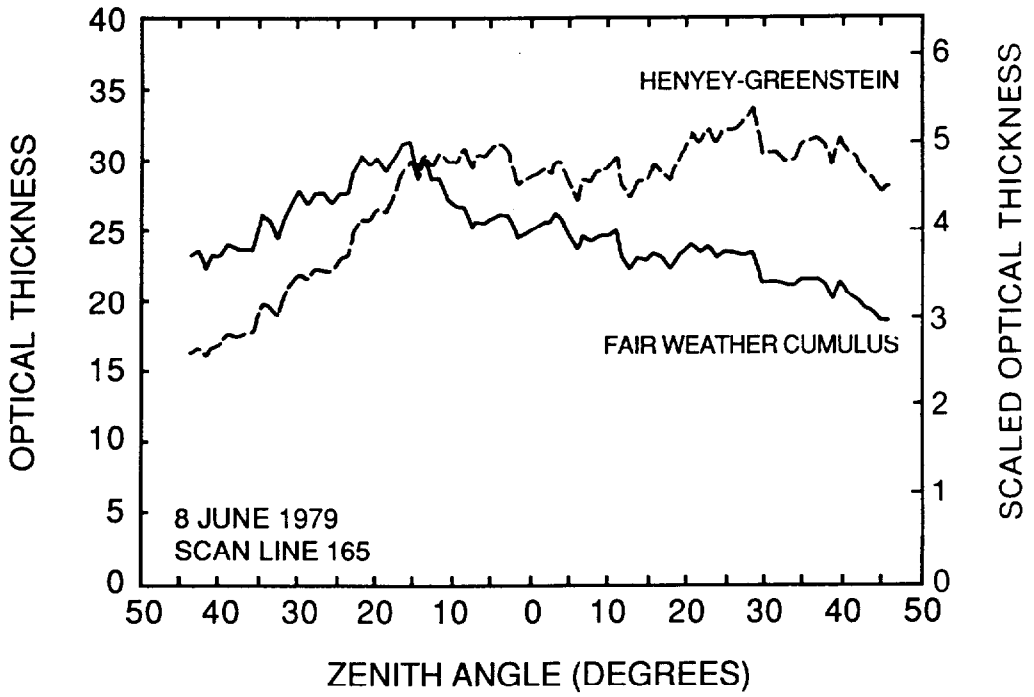

FIG. 10. Optical thickness as a function of zenith angle for scan line 165 of the cloud radiometer on 8 June 1979, flight line 2, where the solid curve applies to the FWC model and the dashed curve to the Henyey–Greenstein model. These results were obtained from the measurements presented in Fig. 8.

be derived using the method previously outlined. As this flight did not contain measurements from the nadir-viewing lidar, it was not possible to quantitatively ascertain the degree of homogeneity of the upper cloud boundary. We relied instead on a qualitative assessment of the degree of homogeneity, based on the spatial variability of the reflection function data.

The most striking feature of these cloud optical thickness results is the fact that the two images look very nearly like mirror images of one other. In particular, the cloud optical thickness derived by assuming the FWC model is generally greater on the left-hand side of nadir, while the one derived by assuming the Henyey–Greenstein model is generally greater on the right-hand side of nadir. This result further illustrates the importance of details of the single-scattering phase function in the analysis of reflected solar radiation measurements, and is not at all dependent on the method used for analysis. The advantage of our method lies both in its computational efficiency and in its ability to highlight the physics behind the radiative transfer process. The results obtained from this analysis are no different than those that would be obtained using a table look-up procedure.

In order to gain further insight into the distribution of cloud optical thickness within the scene, probability density functions have been constructed from the FWC and Henyey–Greenstein images of Fig. 11. These results, presented in Fig. 12, were obtained from approximately 90 000 "pixels" having optical thicknesses in the range $5 \leqslant \tau_c \leqslant 100$, each of which had a spatial resolution of about 60 m. These results show that the distribution of cloud optical thickness on this day was strongly bimodal, with the distribution of optical thicknesses generally displaced toward larger optical thickness when the Henyey–Greenstein phase function is assumed in the analysis. The mean optical thickness is roughly the same for both images ($\sim$34), though the mean optical thickness has little meaning for such a bimodal distribution. For the FWC (Henyey–Greenstein) model, the median optical thickness was 29 (33), with 50% of the pixels lying between 14 and 45 (14 and 50).

In all experimental results presented earlier, we assumed $\omega_0 = 1$ and $A_g = 0.2$. From Table 1, we see that if the surface albedo were equal to 0.0, rather than 0.2, all results presented in Figs. 10–12 would be increased by $\Delta\tau_c = 2.1$. On the other hand, had we assumed that the single scattering albedo were 0.9999, rather than 1.0, half the pixels in Fig. 11 would be increased by $\Delta\tau_c \leqslant 1.1$, with only about one-fourth of the pixels increased by $\Delta\tau_c \geqslant 5.2$. Biases associated with uncertainties in the phase function (and asymmetry factor) can be much larger, as seen on examination of Fig. 11.

8. Summary and conclusions

A method has been presented for determining the scaled optical thickness of clouds from reflected solar radiation measurements. The procedure compares

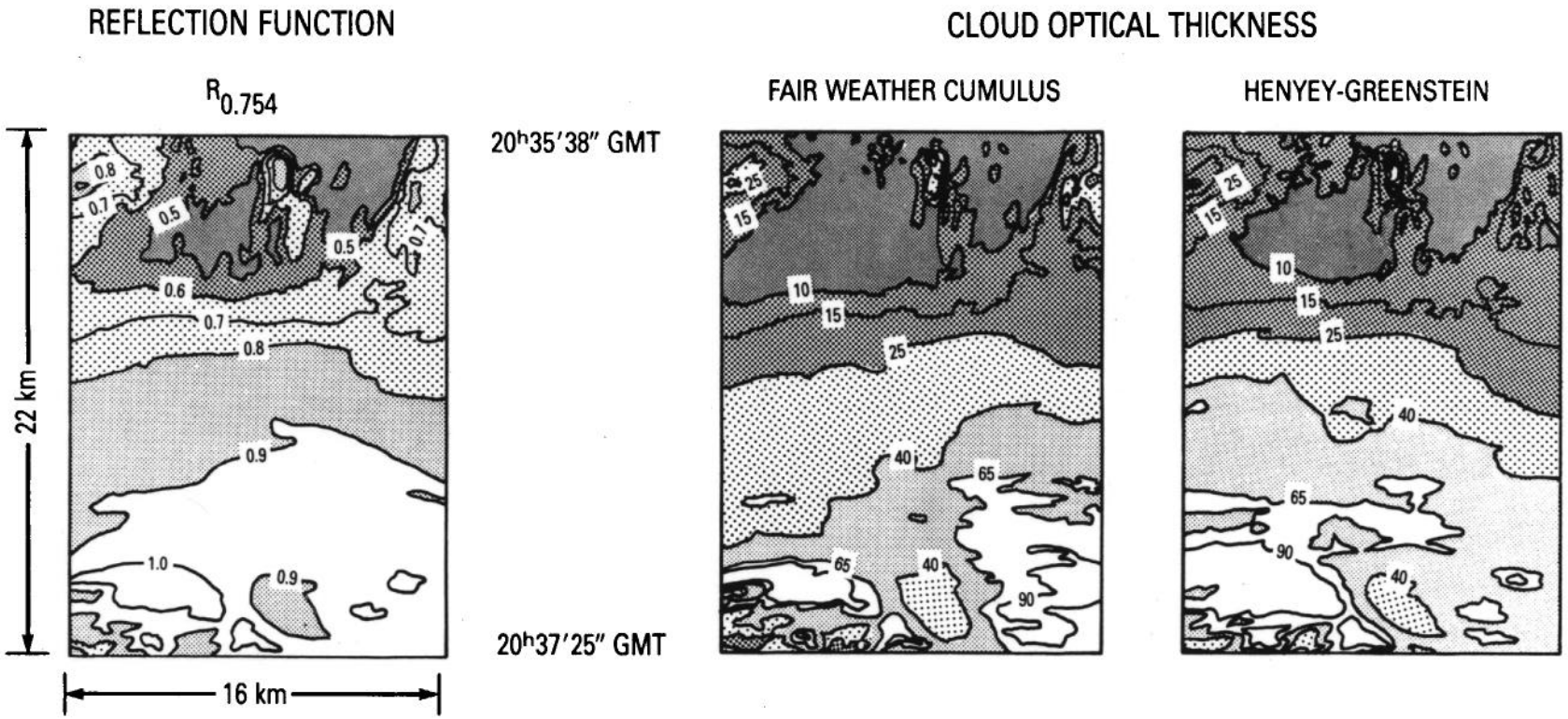

FIG. 11. Images of the measured reflection function and corresponding cloud optical thickness derived from the first 365 scan lines of cloud radiometer data on 8 June 1979, flight line 2. These images have been remapped onto a horizontal grid at 10 km altitude, corresponding to the cloud top altitude of many of the clouds in the scene. The two different cloud optical thickness images result from assuming either a FWC or Henyey–Greenstein phase function in the analysis.

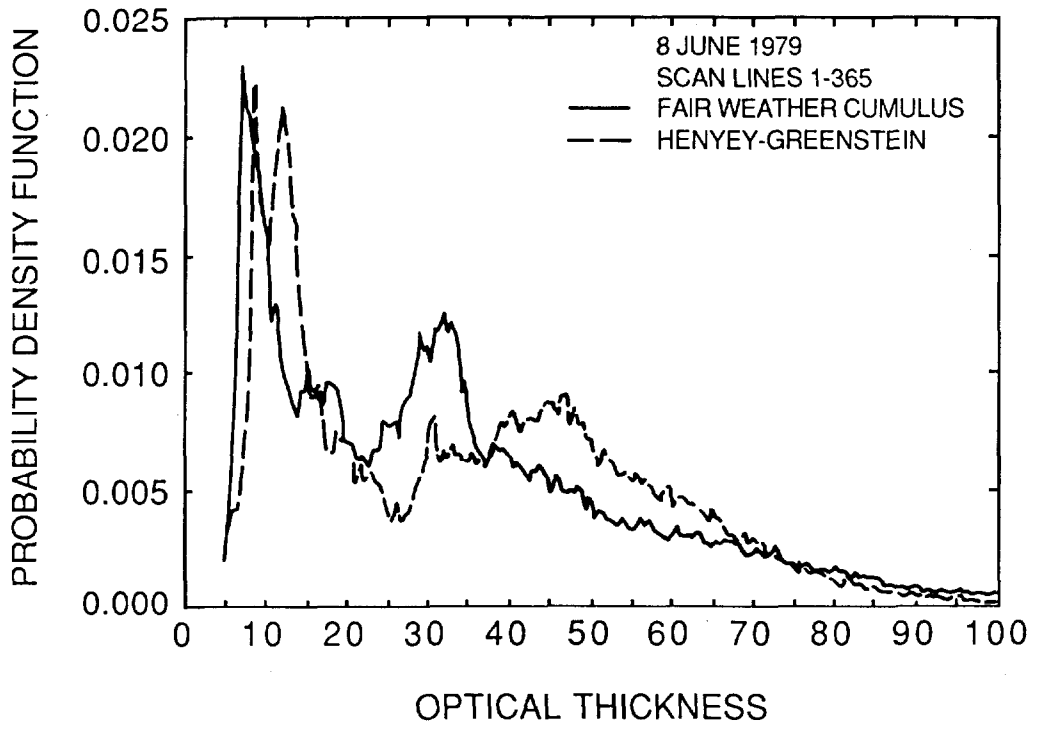

FIG. 12. Probability density function of cloud optical thickness for the 8 June 1979 case presented in Fig. 11, where the solid curve applies to the FWC model and the dashed curve to the Henyey–Greenstein model.

measurements of the reflection function with asymptotic expressions for the reflection function of optically thick layers. Asymptotic expressions for the reflection and transmission functions of thick layers have been derived which show the explicit dependence of the radiation field on cloud optical thickness and surface albedo. In addition, expressions for the reflection and transmission functions of a conservatively scattering atmosphere contain an explicit dependence on cloud asymmetry factor. The dependence of the reflection function on the higher-order coefficients of the Legendre polynomial expansion of the phase function is contained implicitly within the reflection function of a semi-infinite atmosphere. Asymptotic expressions for the reflection and transmission functions of thick layers have been shown to be valid to an accuracy of 1% for scaled optical thicknesses ≥ 1.45 (optical thicknesses ≥ 9), and thus any remote sensing method that makes use of these expressions must necessarily be restricted to optical thicknesses greater than about 9.

By making use of the asymptotic expression for the reflection function of an optically thick, conservatively scattering atmosphere, an expression has been derived which relates the measured reflection function to scaled optical thickness. This expression shows that the effect of surface albedo can be separated from the effect of the measurements, thus leading to a constant bias in the derived cloud optical thickness if an incorrect surface albedo is assumed in the analysis. Furthermore, the optical thickness is shown to depend directly on the *difference* between the measured reflection function and the reflection function of a semi-infinite atmosphere. Since the latter depends somewhat on details of the single-scattering phase function, the derived optical thickness depends on the asymmetry factor as well as higher-order coefficients of the Legendre polynomial expansion of the phase function. Uncertainties in the asymmetry factor alone can contribute to uncertainties in the derived optical thickness of 20%, so uncertainties in excess of 20% are possible even under the conditions of plane-parallel and homogeneous clouds with perfect measurements. Additional uncertainties that arise if the cloud has a small amount of absorption is also considered by making use of asymptotic expressions for reflection from a nonconservative atmosphere overlaying a reflecting surface. The magnitude of such absorption, if present, is presently being examined in a separate experiment (King et al., 1986).

The principal assumption on which the technique is based is that the cloud has a sufficient horizontal extent and horizontal homogeneity to be considered locally plane-parallel. This assumption is independent of our method of analysis, but requires that we restrict our processing to only those portions of experimental data that satisfy this condition. In this paper we have used a subjective criterion of homogeneity based on the variability of the measured reflection function. In the future, nadir viewing lidar data available from the same aircraft platform will permit us to examine the degree of inhomogeneity of the upper-cloud boundary,

as well as to determine whether overlaying cirrus clouds are present. In our analysis, we have further assumed the radiation to be collimated on the upper-cloud boundary, with no diffuse component, such as would arise from moderately thick cirrus clouds.

The efficiency of our asymptotic method for deriving the scaled optical thickness of clouds lies in the fact that the number of terms required in the Fourier expansion of the reflection function of a semi-infinite atmosphere is a strong function of μ and μ_0. This function, denoted $M(\mu, \mu_0)$ and illustrated in King (1983) for both the Fair Weather Cumulus (FWC) and Henyey–Greenstein models, permits the rapid construction of $R_\infty(\mu, \mu_0, \phi)$ using the Fourier expansion given in (10). Since the majority of pixels have small observational zenith angles where few terms are required compared to large observational zenith angles, these computations are quite efficient. For the 8 June 1979 observations discussed in this paper, where $\mu_0 \sim 0.870$, $M(\mu, \mu_0)$ ranges between 0 and 11 for the FWC model (0 and 2 for the Henyey–Greenstein model).

High-resolution images of the reflection function of clouds have been obtained with a multichannel scanning radiometer operated from a high-altitude aircraft. A case study of measurements acquired from a stratiform cloud system has been presented for a sequence of 365 scan lines of data acquired in central Oklahoma on 8 June 1979. These results clearly demonstrate that details of the phase function have an impact on the derived optical thickness of clouds. Although we have emphasized the differences in the derived cloud optical thickness arising from an uncertain knowledge of the cloud phase function, the Henyey–Greenstein phase function is an especially unrealistical phase function for terrestrial water clouds. Thus the differences we find between these two models overemphasizes the errors resulting from phase function uncertainties.

Although our method highlights the physics of the remote sensing method, the results obtained from our analysis are equivalent to those that would be obtained using a table look-up procedure. These measurements and analysis procedures will be continued in marine stratocumulus clouds off the coast of southern California as part of the First ISCCP (International Satellite Cloud Climatology Project) Regional Experiment (FIRE) in 1987.

Acknowledgments. The author is grateful to Drs. R. J. Curran and J. D. Spinhirne for developing the multichannel cloud radiometer used in this investigation and for coordination of field operations of the aircraft. The author is also grateful to H. G. Meyer, G. T. Arnold and K. Govindaraju for software support over the many years required to develop a smooth and efficient data processing, calibration and analysis system. The author would further like to thank the anonymous referees, whose careful reviews and comments led to an expanded treatment of error propagation in the manuscript.

REFERENCES

Ahmad, Z., and R. S. Fraser, 1983: Satellite measurements of cloud reflectance and optical thickness. *Adv. Space Res.*, **2**, 29–34.

Bevington, P. R., 1969: *Data Reduction and Error Analysis for the Physical Sciences.* McGraw-Hill, 336 pp.

Chandrasekhar, S., 1950: *Radiative Transfer.* Oxford University Press, 393 pp.

Curran, R. J., and M. L. C. Wu, 1982: Skylab near-infrared observations of clouds indicating supercooled liquid water droplets. *J. Atmos. Sci.*, **39**, 635–647.

——, H. L. Kyle, L. R. Blaine, J. Smith and T. D. Clem, 1981: Multichannel scanning radiometer for remote sensing cloud physical parameters. *Rev. Sci. Instrum.*, **52**, 1546–1555.

Deirmendjian, D., 1963: Scattering and polarization properties of polydispersed suspensions with partial absorption. *Electromagnetic Scattering,* M. Kerker, Ed., Pergamon Press, 171–189.

Hansen, J. E., 1971: Multiple scattering of polarized light in planetary atmospheres. Part II. Sunlight reflected by terrestrial water clouds. *J. Atmos. Sci.*, **28**, 1400–1426.

——, and J. B. Pollack, 1970: Near-infrared light scattering by terrestrial clouds. *J. Atmos. Sci.*, **27**, 265–281.

——, and L. D. Travis, 1974: Light scattering in planetary atmospheres. *Space Sci. Rev.*, **16**, 527–610.

Henyey, L. C., and J. L. Greenstein, 1941: Diffuse radiation in the galaxy. *Astrophys. J.*, **93**, 70–83.

King, M. D., 1981: A method for determining the single-scattering albedo of clouds through observation of the internal scattered radiation field. *J. Atmos. Sci.*, **38**, 2031–2044.

——, 1983: Number of terms required in the Fourier expansion of the reflection function for optically thick atmospheres. *J. Quant. Spectrosc. Radiat. Transfer,* **30**, 143–161.

——, and Harshvardhan, 1986: Comparative accuracy of selected multiple scattering approximations. *J. Atmos. Sci.*, **43**, 784–801.

——, M. G. Strange, P. Leone and L. R. Blaine, 1986: Multiwavelength scanning radiometer for airborne measurements of scattered radiation within clouds. *J. Atmos. Oceanic Technol.*, **3**, 513–522.

Malkova, V. S., 1973: Use of G. V. Rozenberg's asymptotic expressions for interpretation of cloud brightness measurements. *Izv. Acad. Sci. USSR. Atmos. Ocean. Phys.*, **9**, 548–552.

Rozenberg, G. V., M. S. Malkevich, V. S. Malkova and V. I. Syachinov, 1974: Determination of the optical characteristics of clouds from measurements of reflected solar radiation on the Kosmos 320 satellite. *Izv. Acad. Sci. USSR. Atmos. Ocean. Phys.*, **10**, 14–24.

Spinhirne, J. D., M. Z. Hansen and L. O. Caudill, 1982: Cloud top remote sensing by airborne lidar. *Appl. Opt.*, **22**, 1564–1571.

——, —— and J. Simpson, 1983: The structure and phase of cloud tops as observed by polarization lidar. *J. Climate Appl. Meteor.*, **22**, 1319–1331.

Stephens, G. L., 1978: Radiation profiles in extended water clouds. II: Parameterization schemes. *J. Atmos. Sci.*, **35**, 2123–2132.

Twomey, S., and K. J. Seton, 1980: Inferences of gross microphysical properties of clouds from spectral reflectance measurements. *J. Atmos. Sci.*, **37**, 1065–1069.

——, and T. Cocks, 1982: Spectral reflectance of clouds in the near-infrared: Comparison of measurements and calculations. *J. Meteor. Soc. Japan,* **60**, 583–592.

van de Hulst, H. C., 1968: Asymptotic fitting, a method for solving anisotropic transfer problems in thick layers. *J. Comput. Phys.*, **3**, 291–306.

——, 1980: *Multiple Light Scattering. Tables, Formulas, and Applications.* Vols. 1 and 2, Academic Press, 739 pp.

Wang, J. R., J. L. King, T. T. Wilheit, G. Szejwach, L. H. Gesell, R. A. Nieman, D. S. Niver, B. M. Krupp and J. A. Gagliano, 1983: Profiling atmospheric water vapor by microwave radiometry. *J. Climate Appl. Meteor.*, **22**, 779–788.